PROCEEDINGS, Thirty-Seventh Workshop on Geothermal Reservoir Engineering
Stanford University, Stanford, California, January 30 - February 1, 2012
SGP-TR-194

STRESS HETEROGENEITY AND NATURAL FRACTURES IN THE BASEL EGS GRANITE RESERVOIR INFERRED FROM AN ACOUSTIC TELEVIEWER LOG OF THE BASEL-1 WELL

S. Sikaneta and K. F. Evans
Engineering Geology, ETH Zürich
Sonneggstrasse 5
CH-8092 Zürich, Switzerland

ABSTRACT

Knowledge of the state of stress and the natural fracture system in the subsurface are pre-requisite pieces of information to model and understand the behavior of Engineered/Enhanced Geothermal Systems during stimulation and subsequent operation. This information is also critical to understanding induced seismicity. An ultrasonic borehole image (UBI) log acquired prior to the stimulation of the BS1 well at Basel provides high quality information for characterizing the in-situ stress field and fracture system in the host granite of the reservoir. We present evidence derived from borehole breakouts and drilling induced fractures visible on the UBI log that the stress profile within the BS1 well prior to stimulation displayed a significant level of complexity. We use a new methodology based upon critical stress theory to estimate the minimum and maximum horizontal stress magnitudes. The stress orientation and stress magnitudes fluctuate over the meter to hundreds of meter scales, with fluctuations demonstrably correlated to the occurrence of natural fractures visible on the UBI log. The complexity of the stress field in BS1 contrasts with approximation commonly used in numerical models, that the pre-stimulation state of stress in the subsurface has a constant orientation and magnitudes that vary in a linear manner with respect to depth. These approximations appear valid only in the long-wavelength limit. The findings suggest that the numerical simulation of the EGS reservoir stimulation process using physical models to estimate seismic hazard and permeability creation should include consideration of the complexity of the initial stress conditions

INTRODUCTION

The Basel Deep Heat Mining (DHM) project is located in northwestern Switzerland at the junction of the Upper Rhine Graben and the Jura mountains (Figure 1). The target reservoir for the DHM project is fractured granitic basement that underlies 2600 m of sediment. The site lies within the conurbation of the city of Basel, where there is relatively high heat flow, factors which promoted the development of the project. To date, two deep wells have provided information about the granitic reservoir: Otterbach-2 (OT2), and the Basel-1 (BS1) well. OT2 was drilled as an exploratory well and confirmed a temperature of 107°C at 2,400 m (Häring, 2001). BS1 was drilled as the first well of an EGS duplet in 2006. The well was drilled sub-vertical to 5,000 m, and cased to 4,629 m MD below ground level. The open hole section was subject to a hydraulic stimulation injection in 2006 to promote shear failure and dilation of pre-existing fractures, thus enhancing the permeability of the rock mass. Microseismic events began to be observed when injection pressures were only a few MPa, indicting some fractures were close to shear failure under ambient conditions (Häring et al, 2008). The stimulation operation was prematurely terminated when seismic events that were felt by the local population began to occur, the largest event of M_L = 3.4 occurring after shut-in. The project has subsequently been stopped due to public concern.

The top of the granite at the BS1 site is encountered at 2426 m. The hole was drilled as 14-1/4 inch to 2594 m, and a 10-1/4 inch liner cemented. The hole was then extended as 9-7/8 inch to 4834 m, and 8-1/2 inch to 5000 m. Prior to running the 7-5/8 inch casing to 4629 m, an ultrasonic borehole imaging log (UBI) was run from the 10-1/4 inch lining shoe to total depth of 5 km. The log provides key information about the natural fracture network and the pre-stimulation stress field, two aspects which are reported in this paper.

The UBI log presents two images of the borehole wall: a caliper image and an amplitude image. The caliper image, derived from processing the time taken for ultrasonic pulses to travel from the UBI tool to the formation and back, provides the necessary data to reconstruct the three-dimensional geometry of the borehole. The amplitude, or acoustic reflectivity image provides information about the change in amplitude between the signal sent from the tool and that received. The presence of fractures and changes in rock properties are more readily apparent on the amplitude image than on the caliper image, and

consequently the amplitude image is used to examine the natural fracture system. The caliper image constitutes the main source of information for identifying and characterizing breakouts. Details of the acoustic televiewer logs run in BS1 and OT2 can be found in Valley and Evans (2006).

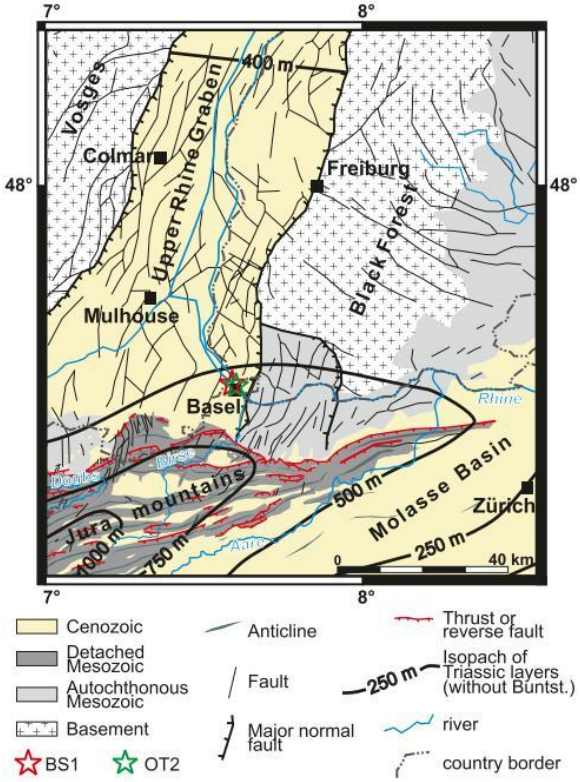

Figure 1: Location of the BS1 and OT2 wells at the southern end of the Upper Rhine Graben (after Valley and Evans 2009).

NATURAL FRACTURE NETWORK

The dip and dip direction of natural fractures was estimated using a procedure that took account of non-circular borehole geometry that was a common feature of the hole (e.g. breakouts are present over some 80% of the log). A routine was written that computed the coordinates of all points along the intersection of a planar fracture of given dip and dip direction with the borehole defined by the caliper log about a given centre depth. The coordinates were then used to project the trace onto the amplitude image where it could be adjusted to give a best fit to observed fracture traces. The procedure yielded estimates of dip, dip-direction and depth of all natural fractures. The resulting distribution of poles to the planes of fractures is shown in the stereographic plot of Figure 2. Three distinct populations are visible. Given that natural and induced seismicity indicates the rock is hosting normal- to strike-slip stress with ENE-WSW orientation for S_3, clusters 1 and 2 could be interpreted as conjugate shear fracture populations. Cluster 1 is sub-parallel to the average orientation of SHmax within the reservoir derived from the analysis of wellbore failure (Valley and Evans, 2006), and also from inversion of focal mechanisms of natural seismicity (Kastrup et al, 2004). The peaks and troughs of fractures in Clusters 1 and 2 occur within the sector of the borehole wall where breakouts tend to occur. This makes it difficult to distinguish natural fractures from drilling-induced fractures forming within the compressional sector, such as incipient breakout fractures, or petal fractures (Plumb, 1989). The orientation distribution shown in Figure 2 differs slightly from that presented in Häring et al (2008) primarily because of an error in dip estimation in the latter analysis. However, the difference is not great.

Fracture density is greatest near the top of the granite and declines with depth as illustrated by Figure 3. This might reflect the fact that the top of the granite is a paleo-weathered surface (Valley & Evans, 2006). Observed natural fractures are clustered together in space. This is evidenced by the the histogram of fracture spacing shown in Figure 4 which conforms to a thick-tailed distribution.

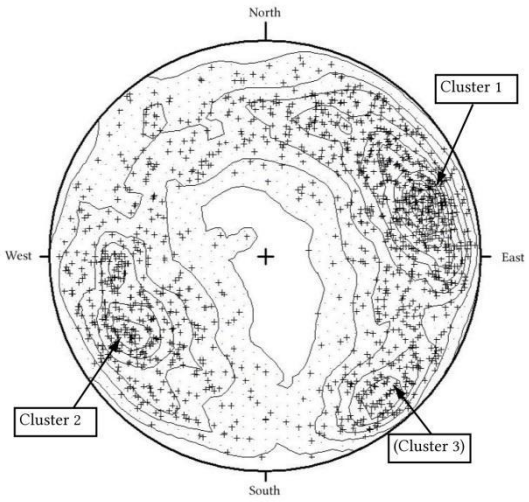

Figure 2: Equal Area Plot (N=1249) of poles to natural fracture planes (after Fabbri, 2010).

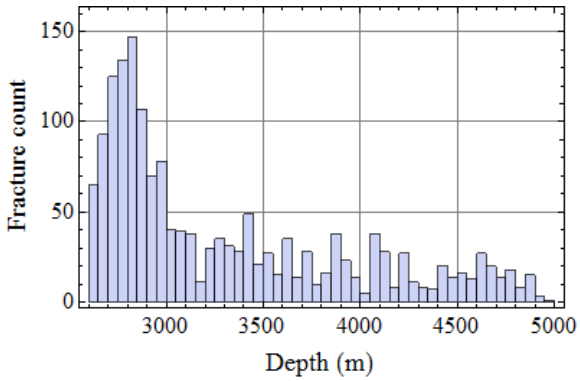

Figure 3: Histogram (N=1249) of natural fracture density with respect to depth. Binning interval is ~42 m.

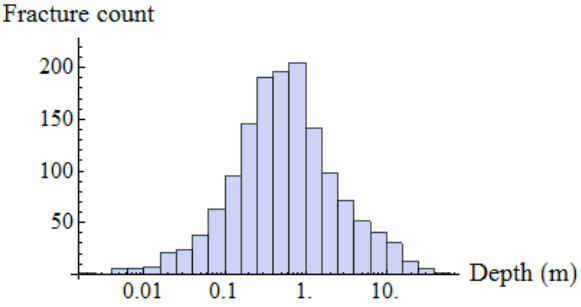

Figure 4: Log histogram (N=1249) of natural fracture spacing.

DRILLING INDUCED TENSION FRACTURES

Drilling induced tension fractures (DITFs) were mapped in a similar manner to the method described for natural fractures. A Bezier curve was fit to the trace of the amplitude image of a DITF and the coordinates of all points along the curve were obtained by projection of the curve onto the caliper image. DITFs are distinguished from natural fractures on the UBI log by their tendency to display a more discontinuous traces across the borehole wall. They also tend to cluster into genetically related sets. For example, axial DITFs, which are parallel to the borehole axis, often evolve into drilling induced petal fractures or terminate against natural fractures. En-echelon fractures are often clearly induced, forming stepped sets of fractures that appear as a herring-bone pattern on the UBI log.

BOREHOLE BREAKOUTS

Borehole breakouts are regions of the well in which compressive stresses at the borehole wall have caused failure. Borehole breakouts provide valuable information for estimating the orientation of in-situ stresses, and also potentially their magnitude. For brittle polycrystalline rocks at low confining pressure, spallation is the most commonly observed failure mode at borehole and tunnel walls. Since the UBI log was run within a granite reservoir, it is most likely that observed breakouts were caused by spallation. Spall fragments were also observed during drilling of the well, further supporting the hypothesis. Some 80% of the 2,400 m of borehole imaged in BS1 suffered breakouts to some degree. In order to make the analysis as objective as possible, an automated routine was developed to detect and measure their occurrence.

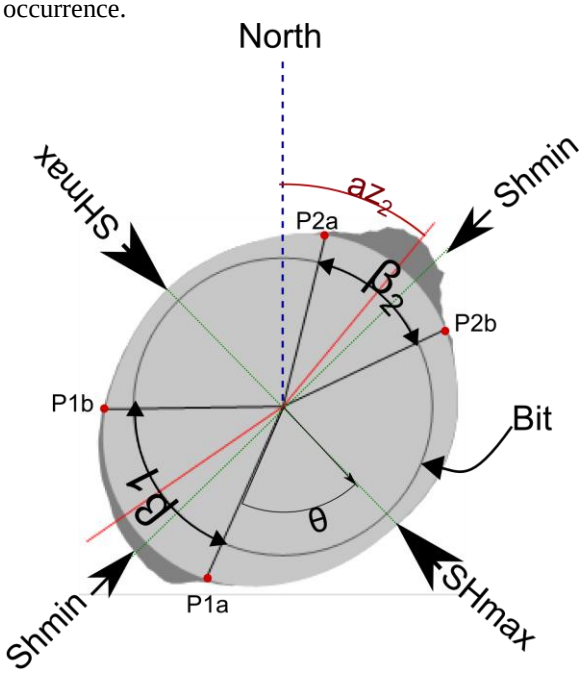

Figure 5: Diagram illustrating borehole breakouts (dark grey areas), definition of breakout widths β_1 and β_2, and the relative orientation of SHmax and Shmin. The light grey area is the region admissible to having been drilled by the bit (shown as a circle). Breakout azimuths are measured from north to the center of each breakout. Stress inversions assume that at points P1a,P1b,P2a, and P2b, the rock is on the verge of failure.

Detecting and measuring borehole breakouts

There are few descriptions in the literature of methodologies used to identify and measure both the orientation and the width of breakouts. Berard and Cornet (2003), describe an automated technique in which it is assumed that the drilled wellbore is a perfect cylinder. Accurate measurement of breakout width, defined by the angle subtended by the breakout zone, β, (Figure 5), is important because stress magnitudes estimated from inversion of the width can be highly sensitive to the latter, inversions based upon borehole breakouts can be highly sensitive to its value, particularly at large angles approaching 120° (Valley, 2002). The difficulty of

detecting and measuring breakouts is exacerbated in enlarged and ovalized holes where it can be difficult to discern the boundary between broken-out and intact regions of the wellbore, as illustrated in Figure 5 in which the borehole is significantly larger than the bit, and is ovalized.

The delineation of broken out zones in our automated routine is accomplished by applying simple kinematic considerations and quality control criteria: all regions of the wellbore cross-section which *could not possibly have been drilled by the bit* are flagged as potential breakout zones. Following this, quality control criteria are used to screen flagged sectors of the cross-section. First, the two largest continuously flagged sectors of the borehole are identified, measured, and accepted as possible breakouts. During this step, the continuity of flagged segments is calculated using a clustering method, the description of which is beyond the scope of this paper. The two largest continuously flagged sections are taken to be a breakout pair if: (a), the larger of the two sections has a width not more than 50% larger than the smaller, and (b), the orientation of the two sections (as given by their center-points) are within 45° of being diametrically opposite each other. The distribution of observed breakout widths is shown in the histogram of Figure 6. Breakout widths in BS1 are relatively large with a mean value of 79.1°. The satndard deviation is ±22.6° if breakout limbs are binned separately, and ±16.1° if averages of the two limbs are taken.

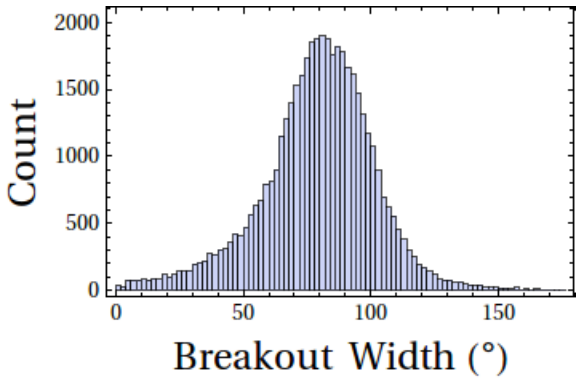

Figure 6: Histogram of breakout widths. The mean width is 7.19° ±22.6° or ±16.1° depending on whether breakout limbs are treated independently or averaged.

STRESS FIELD CHARACTERIZATION

Drilling induced tension fractures (DITFs) seek to open along the path of least resistance and thus perpendicular to the local minimum compressive stress. The strike of DITFs is therefore a measure of the orientation of SHmax, the maximum principal horizontal stress. Breakouts form as a result of compressive failure at the borehole wall and thus occur in a direction orthogonal to the strike of DITFs.

The mean strike of SHmax, obtained from the strike of the axial and en-echelon DITFs imaged in this study is 152° ±11° E of N. This is similar to the value obtained by Valley and Evans (2006) of 151° ±13°.

Horizontal stress orientation from breakout orientation

The center of borehole breakouts is expected to be aligned with the orientation of Shmin, the minimum horizontal principal stress. The mean orientation of Shmax derived from the breakouts measured using the automated method described earlier is 143° ± 12.5° E of N, which is similar to the value obtained by Valley and Evans (2006) using manual picking of 143 °± 14° E of N.

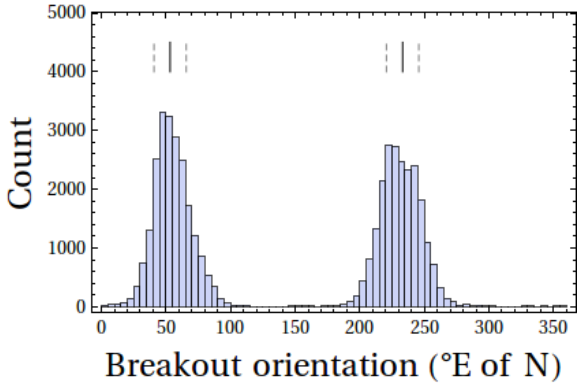

Figure 7: Histogram of breakout orientation in 6° bins. The mean orientation is 53° ± 12.5° E of N, implying an SHmax orientation of 143° ± 12.5° E of N.

Stress Magnitudes from borehole breakouts

The stresses at the surface of an intact circular borehole may be expressed in terms of the far-field stresses if the borehole is drilled parallel to a principal stress and into an elastic formation. In situations where breakouts occur, it is reasonable to hypothesize that within the breakouts, the stresses at the borehole wall have exceeded the strength of the rock, while outside it, the stresses are less than the strength of the rock. The stress state at the edges of a borehole breakout thus lies on the failure envelope. Observations of the locations of breakout edges may thus be used together with an appropriate failure model and linear elastic theory to place constraints on the possible far-field stresses.

The stresses around the borehole are modeled with the following equations for the non-zero components of effective stress at the borehole wall.

1a) $\sigma\theta\theta$=-Pp-Pw+SHmax+Shmin-2(SHmax-Shmin)cos(2θ)
1b) σv=-Pp-+Sv-(SHmax-Shmin)cos(2θ)

1c) σrr =Pw-Pp

In the above equations, σθθ is the tangential effective stress, σv is the vertical effective stress, σrr the radial effective stress, Pw is the wellbore pressure, Pp is the pore pressure, and ν is Poisson's ratio, taken to be 0.25 in this study. θ is the angular co-ordinate measured in a clockwise direction from the direction of SHmax towards Shmin.
Since the phenomenon under consideration involves compressive failure, the effective stress law that is used is that appropriate for compressive failure: e.g. σθθ = Sθθ- Pp, where Pp is pore pressure. The implicit effective stress coefficient of 1.0 is appropriate for the long term compressive failure of low porosity, brittle crystalline rocks (Vernik, 1992).

Two stress inversion methodologies based upon breakout width were used to estimate the magnitude of the stresses. One is the common method where Shmin is known and SHmax is solved for. The second assumes the stresses in the rock mass are everywhere in a critical state. This assumption allows both SHmax and Shmin to be solved for. Both of these methods require on a model of the rock strength.

Rock Strength models

Rock strength does not have a single value but rather is a complex function of the magnitude and orientation of the stresses acting on the rock as well as a variety of environmental factors such as temperature and fluid chemistry. Chemical and thermal effects are neglected in our analyses, resulting in conservative (lower) estimates of the stress magnitudes from borehole breakouts. We assume that the strength and elastic properties of the granite are elastic, allowing the strength of the rock to be described generically as

2) $F(S3,S2,S1) = 0$

Where S1>S2>S3 are the maximum, intermediate and minimum principal stresses respectively, and *F* is a failure criteria function. The importance of using a failure model that accounts for all three principal stresses in problems of borehole mechanics has been highlighted by a number of authors including Vernik and Zoback (1992), Haimson and Chang (2000), You (2009), and Ajmi (2006), amongst others. We have used two models of rock strength to estimate stress magnitudes; a maximum stress criterion in which failure depends on the value of only one of the three principal stresses, and an empirical true-triaxial (ETT) failure criterion that relies on all three principal stresses. The Mohr-Coulomb failure criterion, a commonly used criterion in rock mechanics that depends upon the maximum and minimum principal stresses, reduces to the maximum stress criterion for the problem of a wellbore with no filter cake under hydrostatic conditions and an effective stress coefficient of 1.0, since under these conditions the effective radial stress at the borehole wall is zero.
Figure 8 shows fits of the Mohr-Coloumb and ETT criteria to the results of triaxial compression tests performed on the Basel granite by Braun (2007).

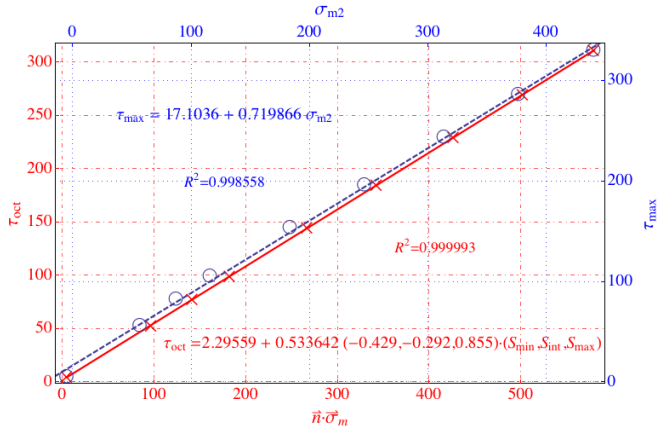

Figure 8: Fits of standard triaxial test data to Mohr-Coulomb and ETT failure criteria.

.
The ETT criterion relates the (octahedral) shear stress at failure to a rock-dependent, linear combination of the principal stresses. In the ETT model two scalars, a and b, and a unit vector $\vec{n} = (n_{s3}, n_{s2}, n_{s1})$ are related to τ_{oct} , the octahedral stress at failure:

(3) $$\tau_{oct} = a + b[\vec{n} \cdot (s_{31}, s_2, s_1)]$$

The validity of this model in describing true-triaxial results has been confirmed using published datasets and will be presented elsewhere. We note that a number of well-established failure criteria such as the Drucker-Prager (1952), Mogi (1967), and Mogi (1971), criteria are specific forms of Eq. (3). The ETT criterion is a "bona fide" true-triaxial criterion that requires true-triaxial test data for proper calibration. To avoid this requirement we have assumed that the ratio between components of $\vec{n}$ that relate the intermediate and minimum principal stresses at failure, have a similar relative value to that given by fitting the ETT criteria to compiled true triaxial tests on Westerly granite given by Ajmi (2006). The fitting error using this assumption is very low, with an R^2 value of essentially 1. The ETT criteria gives lower error, on average, at predicting the maximum stress at failure, than does the Mohr-Coulomb criteria. However, at low confining stresses the error is greater that the MC criteria.

Stress magnitudes assuming a linear minimum stress profile

Häring *et al.* (2008) provide a linear stress profile for BS1 based upon estimates acquired from three depths. Lower bound estimates were obtained from a cement/formation integrity test performed at 2594 m, and the maximum injection pressure at the top of the open hole section at 4629 m during stimulation. The third estimate stems from a RACOS© (Braun, 2007) study based on cores taken at 4900 m that provides an estimate of the minimum and maximum horizontal stresses at that depth. It is difficult to confirm the accuracy of the presented stress profiles since the formation integrity test provides only a lower bound on the minimum horizontal stress, and the RACOS method, which is based upon microcrack-induced seismic anisotropy of small samples, is proprietary.

If the Shmin and Sv profiles given by Häring *et al.* (2008) are taken as correct, and the rock strength model is valid at all depths, then observed variations in breakout widths must be due to Shmax variations.

It is reasonable to take the vertical stress as equal to the overburden stress. Häring *et al* (2008), provide the following relationship, derived from density logs, of the relationship between the depth z (in m) and the vertical stress Sv:

(4) Sv[MPa] = 0 0.0249 z[m]

The formation fluid density used in the calculations was 1.03 g/cc. There was no mud-cake present, wellbore pressure, Pw, was taken as pore pressure. There is thus only one unknown stress component, SHmax, in Eq (1).

The constraint that the stress state at the edges of the breakouts lie on the failure envelope leads to a determinable solution for the unknown stress magnitude. The edges of the breakouts measured clockwise from the SHmax direction are $\theta = (90° \pm 0.5\beta)$, where β is the breakout width defined earlier (Figure 5). Figures 9a to 9b show the computed SHmax profiles for BS1 using the two rock strength models and this methodology.

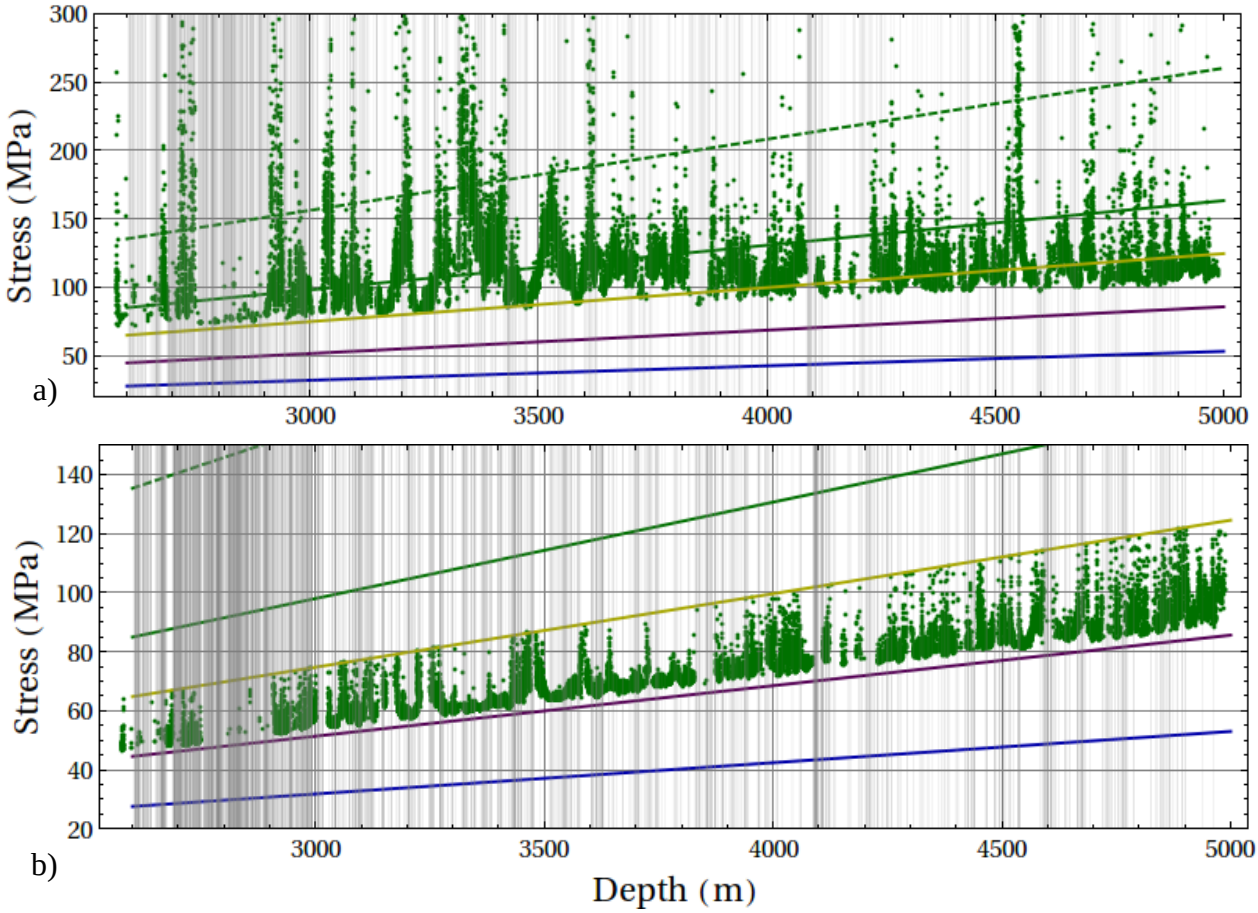

Figure 9: Predicted SHmax profiles derived from breakout widths using the linear trends for Shmin and Sv given by Häring et al (2008) and rock strength given by (a) the maximum stress criterion, and (b) the ETT criterion. Blue is pore pressure, magenta is Shmin, lime green is Sv, and the dark green solid and dashed lines are the lower and upper limits of SHmax given by Häring et al. The vertical lines denote the locations of natural fractures and fracture zones.

Using the maximum stress criteria and the experimentally measured uniaxial compressive stress of 113 MPa results in a SHmax gradient of 38.8 kPa/m with a high standard of deviation of 355 kPa/m. The ETT criterion gives a much lower mean gradient of 19.1 kPa/m and with a standard deviation of 1.2 kPa

Stress magnitudes assuming a critically stressed reservoir

Since the range of uncertainty associated with the linear stress profiles given by Häring *et al.* (2008) is large, and the data set has little resolution, an alternative method of estimating the range of stresses present in the reservoir was sought. Critical stress theory suggests that in most places within the earth's crust, optimally oriented fractures are in a state of incipient failure. This hypothesis appears to be valid on average within the Basel reservoir since the injection pressure required to induce slip as indicated by seismicity was of the order of a few MPa, two orders of magnitude lower than the approximate stress levels at the reservoir depth.

Critical stress theory predicts a constant ratio between the maximum and minimum principal effective stresses that is dependent on the friction coefficient of fractures, μ_f. If an effective stress coefficient for compressional failure of 1.0 is used, and cohesion on the pre-existing fractures is negligible, then, at the point of failure, S1 and S3 are related by (Zoback, 2007):

$$S1 = Pp + (S3-Pp)\left(\left(1+\mu_f\right)^{0.5} + \mu_f\right)^2 \quad (5)$$

If the critical stress assumption holds in the vicinity of the wellbore (i.e. within 5 diameters or ~ 1.2 m in the case of BS1), and the value of μ_f is known or can be bounded, then Eq. (5) can be used to reduce the number of unknown stresses in Eq. (1) by one. The state of stress at the edge the breakouts is then solvable given one of the two rock strength models. We computed stress magnitudes for BS1 using this approach for μ_f values of 0.6, 0.8 and 1.0, and the two rock strength models. These results are illustrated on the following pages.

The results of our stress inversion are given in Tables 1 and 2. Table 1 gives the percentage of points along the profile where the estimated value of SHmax exceeds Sv (i.e. strike-slip regime). All other points correspond to a normal faulting regime. Evidently, the maximum stress criterion predicts a strike-slip regime, whereas the ETT criterion predicts a normal stress state (see Table 1.). This holds for all reasonable values of μ_f. The ETT criterion leads to significantly lower estimates of SHmax than the maximum stress criterion.

Table 1: Percentage of inversion results using the critical stress methodology that lead to Shmin<Sv<SHmax, (i.e a strike slip regime). All other inversions yield normal regimes (i.e. Shmin<SHmax<Sv)

Criterion	μ_f	% Strike-Slip inversions
SMAX	0.6	85.0
SMAX	0.8	87.5
SMAX	1.0	87.3
ETT	0.6	2.7
ETT	0.8	7.1
ETT	1.0	11

Table 2 shows the depth trends of SHmax and Shmin predicted by the various models. The trends were computed by taking the average of the ratio of the stress component at a depth divided by that depth. The gradients given by Häring et al are given for comparison. All gradients of Shmin are less or equal to the value of Häring et al. The estimates of SHmax from the maximum stress criterion are similar to the lower bound of Häring et al, but the estimates from the ETT method are much lower

Focal mechanisms of natural and induced seismicity at Basel indicate that the stress regime is indeed mixed between strike slip and normal. We observe that assuming a higher friction coefficient results in a larger standard deviation in stress estimates and higher stress gradients for SHmax, and lower stress gradients for Shmin. Table 2 summarizes these trends.

Table 2: Mean and standard deviation of stress gradients computed using the critical stress method.

	Criterion	μ_f	Gradient Mean kPa/m	Standard Deviation kPa/m
Shmin	Häring et al (2008)	-	17.1	-
SHmax	Häring et al (2008)	-	32.7 to 52.0	-
Shmin	SMAX	0.6	17.2	1.9
SHmax	SMAX	0.6	31.0	6.2
Shmin	SMAX	0.8	15.7	1.8
SHmax	SMAX	0.8	32.6	8.0
Shmin	SMAX	1.0	14.6	1.6
SHmax	SMAX	1.0	33.5	9.8
Shmin	ETT	0.6	15.2	0.148
SHmax	ETT	0.6	19.7	1.85
Shmin	ETT	0.8	13.9	0.237
SHmax	ETT	0.8	20.6	2.61
Shmin	ETT	1.0	13.1	0.280
SHmax	ETT	1.0	21.2	3.22

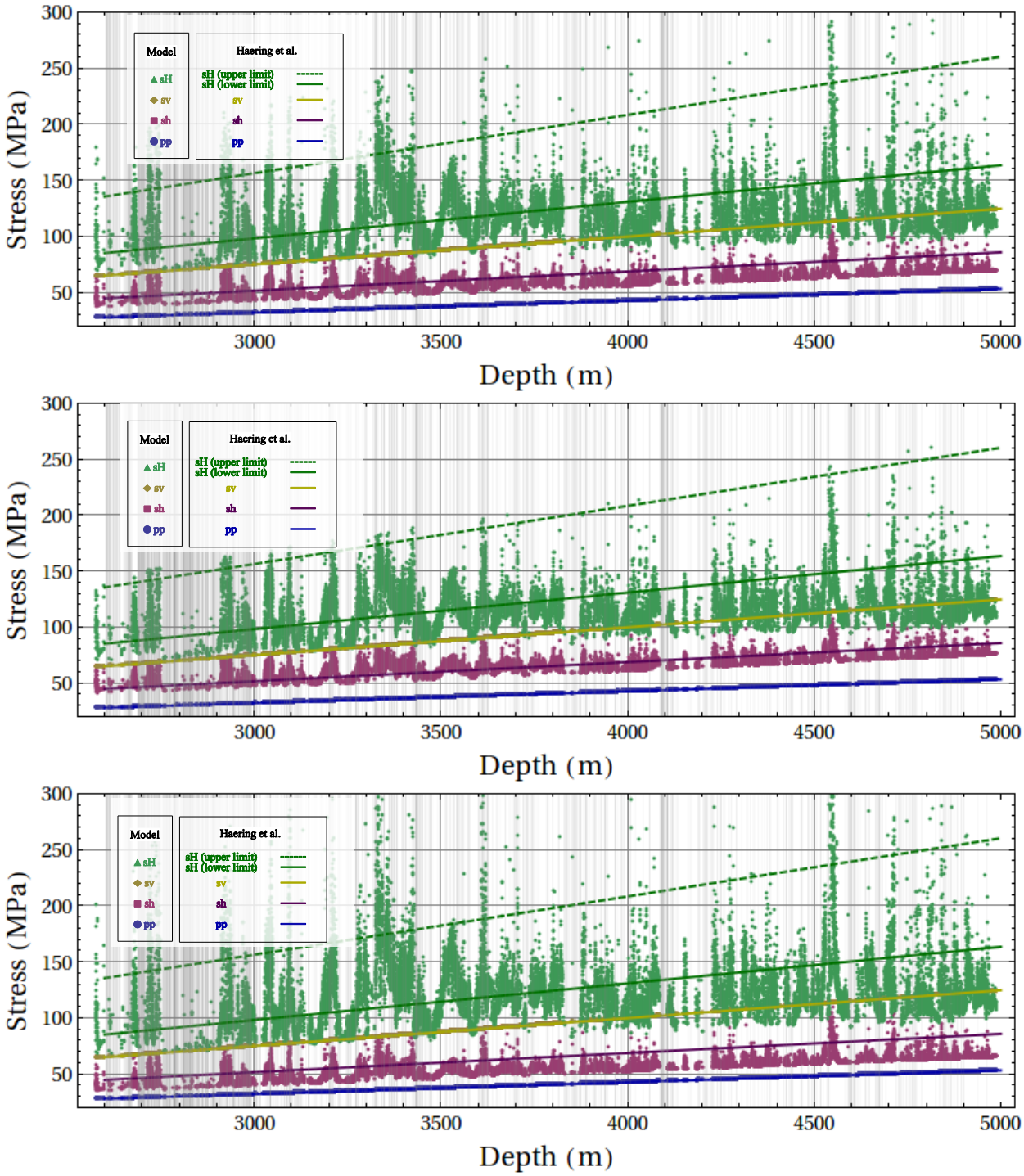

Figure 10: Stress profiles computed using breakout width, maximum stress criterion (UCS =113 MPa), and critical stress theory. Top: μ_f = 0.6, middle μ_f = 0.8, and bottom μ_f = 1.0.

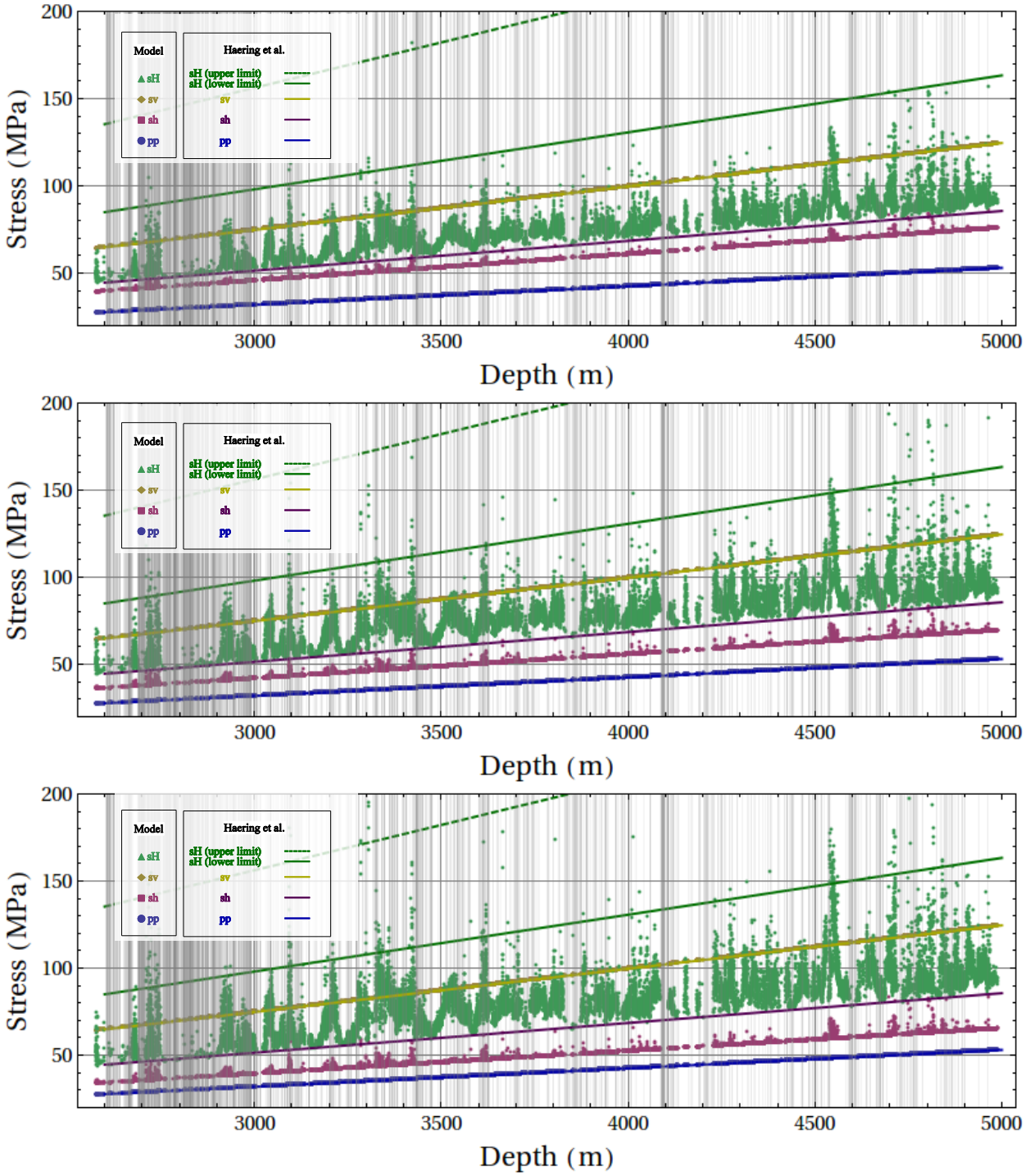

Figure 11: Stress profiles computed using breakout width, ETT strength criterion, and critical stress theory. Top: μ_f=0.6, middle μ_f =0.8, and bottom μ_f = 1.0.

CORRELATION BETWEEN THE LOCATION OF NATURAL FRACTURES IN BS1 AND CHANGES IN THE STRESS FIELD

The displacements associated with shearing and opening of fractures cause a change to the stress field in their vicinity. These changes are particularly pronounced in brittle elastic materials such as granite. It can thus be expected that some of the changes in the orientation and magnitude of the stress field within BS1 should be correlated to the occurrence of natural and/or drilling induced fractures. Figures 12 to 14 present examples of such correlations. In these figures orange points superimposed upon the amplitude log show the location of breakout edges detected using our automated routine, red points indicate the center of breakouts, and cyan lines the calculated mean orientation of Shmin. At a depth of 3073 m on Figure 12 there is a sudden change in breakout orientation where a fracture intersects the well. Not all fractures are correlated with a change in the stress field orientation. Some, such as the dominant fracture at 3193 m in Figure 12, affect the breakout width more than the orientation, others seems to have no effect upon breakout width or orientation. Figure 13 illustrates stress variations at a slightly larger scale of decameters rather than meters. The longer wavelength disturbances are associated with larger fracture zones denoted by the dark bands crossing the image. The effect of the fracture zone at 3020 m upon breakout orientation and arrest is particularly clear. It is also evident from Figures 11 to 13 that very long wavelength changes to the inverted stress magnitudes are correlated to fracture density.

These observations corroborate the findings of Day-Lewis et al (2010), and Valley and Evans (2010), and Blake and Davatzes (2011) of fracture-correlated changes to stress orientation in crystalline rocks.

DISCUSSION AND CONCLUSIONS

It is clear from observation of the UBI image log that there are significant variations in stress orientation within the Basel reservoir, and that these variations correlate with natural fractures. Similar results have been observed in both the Coso and Soultz geothermal fields and such behavior is predicted by basic mechanics. Provisional results of inversions of breakout width to constrain stress magnitudes in the Basel reservoir show a similar pattern, although there remains considerable uncertainty regarding absolute magnitudes. The primary difficulty is set by the limited constraints that can be placed on the profile of Shmin. We have used critical stress theory together with observations of breakout widths to estimate the stress magnitudes. The results also indicate that there are significant deviations of the stress magnitudes from linear trends with depth, and in many cases the perturbations are correlated with the location of natural fractures.

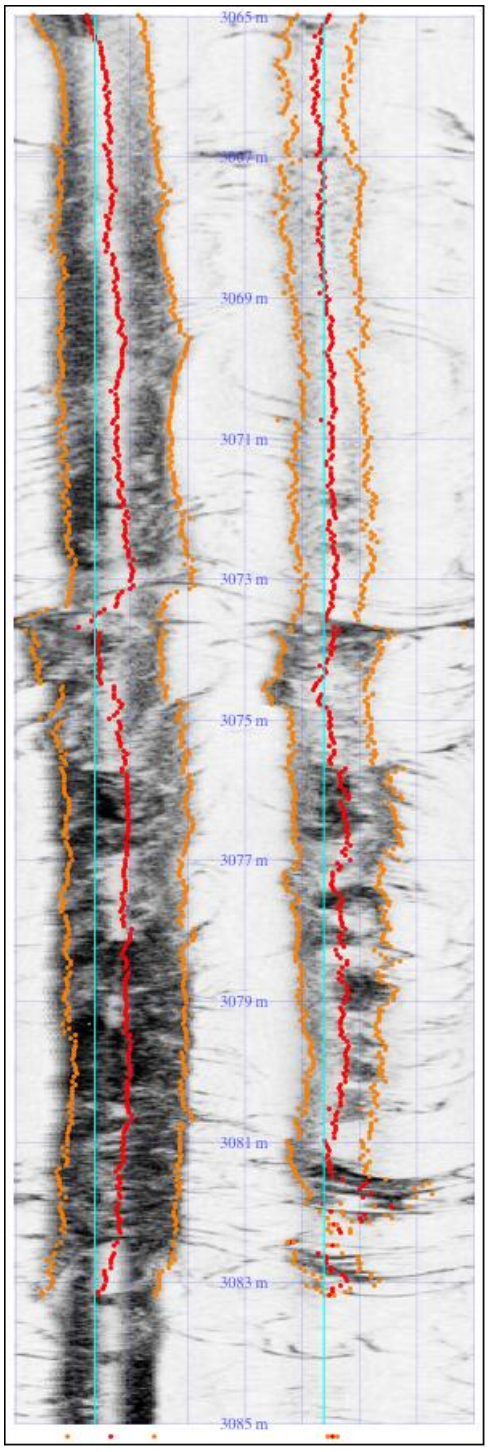

Figure 12: UBI amplitude image in the vicinity of a stress orientation-perturbing fracture at 3073 m. Orange dots mark breakout edges, red dots breakout centers.

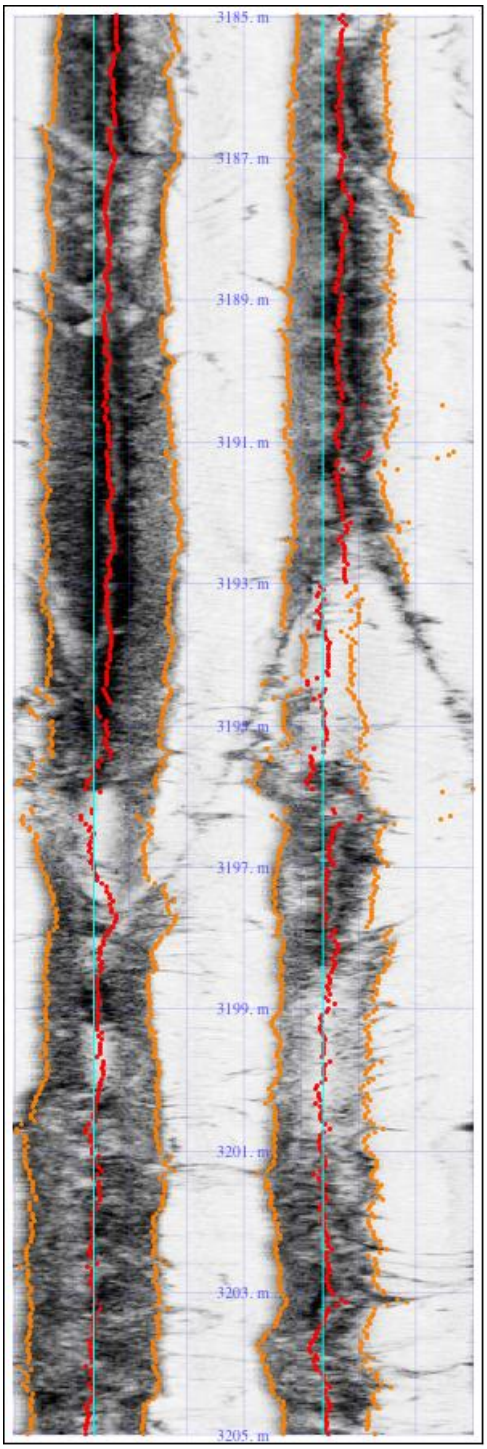

Figure 13: UBI amplitude image in the vicinity of a breakout width/stress magnitude - perturbing fracture at 3195 m. Orange dots mark breakout edges, red dots breakout centers.

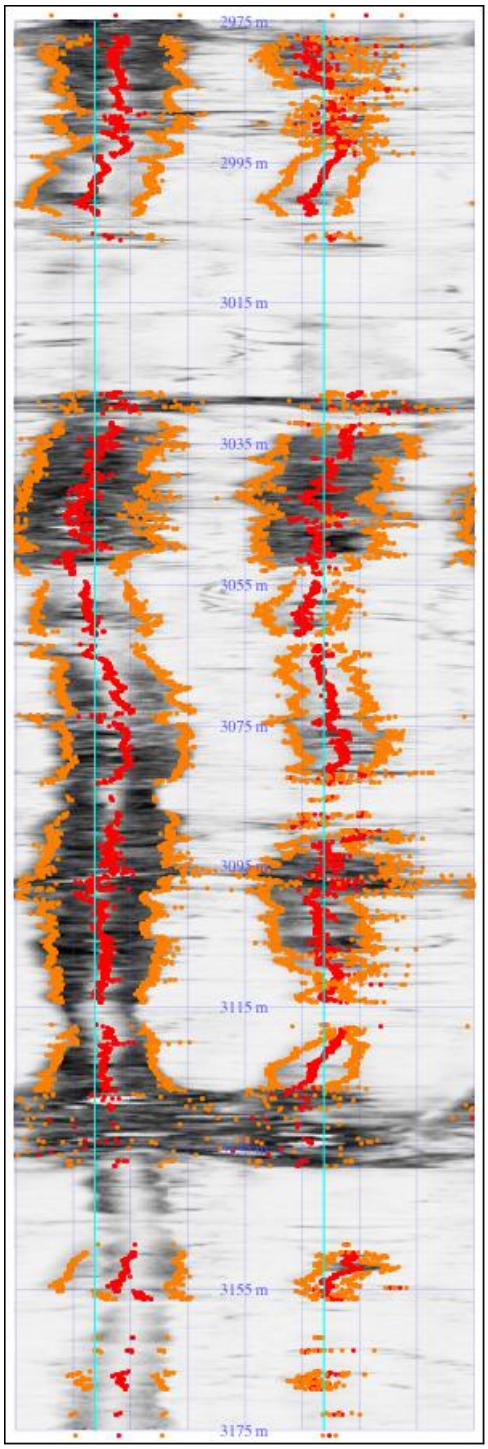

Figure 13: UBI amplitude image in the vicinity of stress perturbing fracture zones (dark bansd cutting across the image at 3025 m, 3095 m and 3135 m. Orange dots mark breakout edges, red dots breakout centers.

ACKNOWLEDGEMENTS

The work was performed as part of the GEOTHERM project that is funded by the Competence Centre for Environment and Sustainability of the ETH-Domain, and by the Swiss Federal Office of Energy under contract 154278. We are grateful to Geopower-Basel and GeoEnergy-Suisse for providing access to the data.

REFERENCES

Ajmi, A-A. (2006), "Wellbore Stability Analysis Based upon a New True-Triaxial Criterion", *PhD. Thesis*, KTH, Sweden.

Berard, T., and Cornet F. (2003), "Evidence of thermally induced borehole elongation: a case study at Soultz, France." *International Journal of Rock mechanics and Mining Sciences*, **40**,1121-11140.

Blake, K., and N. Davatzes (2011), "Crustal stress heterogeneity in the vicinity of COCO geothermal field, CA.", paper presented *at 36th Workshop on Geothermal Reservoir Engineering*, Stanford University, Stanford University, Jan31-Feb2.

Braun., R., (2007) *Analyse gebirgsmechanischer Versagenszundstände beim Geothermieprojekt Basel*. Report to Geothermal Explorers LTD. Basel, Switzerland.

Day-Lewis, A., M. Zoback, and S. Hickman (2010), "Scale-invariant stress orientations and seismicity rates near the San Andreas Fault", *Geophys. Res. Lett.*, **37**(L2434), pp 5.

Drucker, D. C. and Prager, W. (1952). "Soil mechanics and plastic analysis or limit design." *Quart Appl Math*, **10**, 157-165

Fabbri, S. (2010), "Correlation of Stress Variations and Natural Fractures in the Basel Geothermal Borehole (Switzerland)," *B.Sc Thesis*, ETH Zurich, Switzerland.

Haring, M.O. and Schanz, U. and Ladner, F. and Dyer, B.C. (2008), "Characterisation of the Basel 1 enhanced geothermal system," *Geothermics*, **37**,469-495.

Häring, M. (2001), Technischer Bericht Geothermie-Sondierbohrung Otterbach 2, Basel, Geothermal Explorers Ltd.

Haimson, B.C., and Chang, C. (2000), "True triaxial strength and deformability of the German Continental Deep Drilling program (KTB) deep hole amphibolite." *Journal of Geophysical Research*, **107**,B8, 2257,18999-19

Kastrup, U., Zoback, M.L.,Deichmann, N., Evans, K.,Giardini, D. and Michael, A.J., (2004), "Stress field variations in the Swiss Alps and the northern Alpine foreland derived from inversion of fault plane solutions*", Journal of Geophysical Research*, **109**, B01402

Mogi, K., (1967). "Effect of the intermediate principal stress on rock failure". *Journal of Geophysical Research* **72**,5117-5131.

Plumb., R.A, Maury and Fourmaintroux, (*editors)*, Plumb., R.A, (1989), "Fracture patterns associated with incipient wellbore breakouts" in *Rock at Great Depth*, Balkema, Rotterdam.

Valley, B., and Evans K.F. (2009), "Stress orientation to 5 km depth in the basement below Basel (Switzerland) from borehole failure analysis," *Swiss Journal of Geoscience*, **102**, 467-480.

Valley, B., and K. F. Evans (2010), Stress Heterogeneity in the Granite of the Soultz EGS Reservoir Inferred from Analysis of Wellbore Failure, paper presented at World Geothermal Congress, International Geothermal Association, Bali, 25-29 April 2010.

Vernik, V., and Zoback, M.D. (1992), "Estimation of Maximum Horizontal Principal Stress Magnitude From Stress-Induced Well Bore Breakouts in the Cajon Pass Scientific Research Borehole" *Journal of Geophysical Research*, **97**, 5109-5119

You, M.. (2009), "True-triaxial strength criteria for rock" *International Journal of Rock Mechanics and Mining Sciences*, **46**, 115-127.